Proceedings of the 2007 IEEE Symposium on Computational Intelligence in Image and Signal Processing (CIISP 2007)

An Automatic Wavelet-Based Approach for Lung Segmentation and Density Analysis in Dynamic CT

Omid Talakoub[1], Emma Helm[2,3], Javad Alirezaie[1,4], Paul Babyn[2,3],Brian Kavanagh[5], Francesco Grasso[5] and Doreen Engelberts[5]
[1]Department of Electrical and Computer Engineering, Ryerson University, Canada
[2]Department of Medical Imaging, The Hospital for Sick Children, Toronto, Canada
[3]Department of Medical Imaging University of Toronto, Canada
[4]Department of Systems Design Engineering, University of Waterloo, Canada
[5]Department of Critical Care Medicine, The Hospital for Sick Children, Toronto, Canada
otalakou@ryerson.ca, javad@ryerson.ca, paul.babyn@sickkids.ca

***Abstract*— Acute respiratory distress syndrome (ARDS) can occur in people with or without previous lung disease. Analysis of aeration in artificial ventilation for ARDS is one of the major applications of Computed Tomography (CT) lung density examination. A movie of an affected rabbit lung over the respiratory cycle was produced by dynamic CT with a cine loop technique. This technique can produce thousands of CT images for analysis with a single experiment. A fully automated algorithm based on the capability of wavelet transformation to detect edges in the image is proposed. This method accurately and consistently segments the lung in pulmonary CT images. The speed and accuracy of this technique allows it to outperform other methods when dealing with the large number of images created by dynamic Computed Tomography.**

I. Introduction

Computed tomography (CT), originally known as computed axial tomography (CAT or CT scan) uses X-rays to make detailed pictures of structures inside of the body. CT is one of the best tools for studying the chest and lungs. Dynamic CT involves repeatedly imaging the organ of interest over time. This technique can generate thousands of CT images for analysis with a single experiment. Manual segmentation of each study image is very time consuming. Fast automatic segmentation of the lung and subsequent evaluation of its respective density is a prerequisite for any clinical application of this technique. Several studies have examined dynamic CT images of thoracic organs such as the heart [1], [2], [3] and solitary pulmonary nodules [4].

Although CT of the chest is a well established diagnostic method for lung disease, its use in quantification is more recent. In quantitative CT, maps are created of the normalized x-ray attenuation (Hounsfield Units (HU)) of all the pixels in the CT image. The Hounsfield Unit of a given region of lung is proportional to its aeration, for example -500 HU means that the region is composed of 50% lung tissue and 50% air whereas -950 HU means that the lung region is composed of 5% lung tissue and 95% air. By convention, lung aeration can be quantified into 4 categories: 1) normal aeration (-900 to -500 HU), 2) overinflation (less than -900), 3) reduced aeration (-500 to -100 HU) and 4) nonaeration (greater than -100 HU) [5], [6]. It is possible to calculate the volumes of lung in each category by summating the number of pixels within each range multiplied by the area of the pixel and by the CT slice thickness. This is termed lung density analysis or CT densitometry.

Current clinical applications of CT lung density analysis include the assessment of emphysema and the analysis of aeration in artificial ventilation for Acute Respiratory Distress Syndrome (ARDS). Several methods have been proposed to segment the lung in thoracic CT images such as watershed transformation and region growing. However, these methods have drawbacks when it comes to segmenting lung affected with ARDS due to the existence of collapsed regions within the lung. These collapsed regions often have similar density to surrounding soft tissue and maybe erroneously segmented out. Developing a fast and accurate segmentation method is vital for lung density analysis of dynamic pulmonary CT images.

Acute Respiratory Distress Syndrome is a form of acute lung injury of multiple etiologies including pneumonia, sepsis, severe trauma and blood transfusions. Pathologically it is characterized by diffuse alveolar damage with epithelial and endothelial damage, pulmonary edema, inflammatory exudates and cellular proliferation. The typical CT appearance of ARDS is of bilateral ground-glass opacification with a gravity-dependent gradient and atelectasis/consolidation most commonly in the middle and basal parts of the lungs. Artificial ventilation is the mainstay of treatment for ARDS. Many different methods of ventilation have been used to try and optimize oxygenation whilst minimizing lung injury. Quantitative CT has been shown to be a useful method for comparing different types of artificial ventilation to show the effect on lung aeration. Ideally ventilation methods reduce the amount of underinflated (atelectatic) and the amount of overinflated lung with a corresponding increase in the amount of normally aerated lung. Such redistribution of lung aeration has been shown to produce corresponding improvements in oxygenation [7], [8]. As an example normal lung and lung affected with ARDS are illustrated in figure 1.

Traditionally ARDS has been assessed with breath-hold images taken in suspended inspiration or expiration. However, there are several disadvantages of this technique. Firstly,

1-4244-0707-9/07/$25.00 ©2007 IEEE

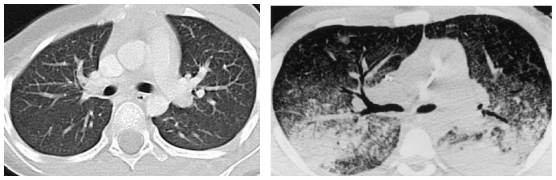

(a) (b)

Fig. 1. (a) Healthy lung (b) affected lung by ARDS.

images taken in suspended respiration do not reflect aeration over the complete respiratory cycle. In addition the act of suspending respiration may alter the aeration of the lung for example by opening up (recruiting) alveoli in inspiration or collapsing (derecruiting) alveoli in expiration. Dynamic CT with a cine loop technique can generate multiple scans of the same area over a defined time period of 100 to 200 milliseconds. This produces a movie of the lung over the respiratory cycle and enables a non-invasive and physiological study of ventilation without the need for breath-holding. It is then possible to examine changes in the volume of atelectatic and ventilated lung as they vary with time and to see how they inter-relate. Such temporal changes can also be used to compare different types of artificial ventilation [9].

II. LUNG SEGMENTATION

The first step is the segmentation of an individual organ of interest in a series of images. Several methods have been developed to segment the lung in pulmonary CT images including thresholding [10], watershed transformation [11], active contours [12], and region growing. Each has its own drawbacks. Thresholding is the most popular lung segmentation method because it is one of the simplest in methodology and computation. In this methodology, each CT voxel[1] can be divided into 2 major types, 1) voxels within the body soft tissues including the chest wall structures (the body voxels) and 2) low-density voxels in the lungs or in the air surrounding the body of the subject (the nonbody voxels). CT lung density is influenced by factors such as subject tissue volume, air volume, image acquisition protocol, physical material properties of the lung parenchyma, and degree of inspiration. These factors make the selection of a single gray-level segmentation threshold difficult, as different thresholds are likely required for different subjects. Although some methods have been proposed based on finding an adaptive threshold value, these methods still have some misregistrations in their segmentation results including missing boundaries between 2 different anatomic regions when there is not a significant discontinuity between them. Most importantly, thresholding schemes may not perform well in ARDS cases since some air sacs fill with fluid and others collapse. Fluid and collapsed air sacs have HU values close to vessels, while threshold schemes pick a value close to air (-1000HU) as lung region. Consequently, collapsed areas would be considered as body voxels rather than collapsed lung.

[1]A voxel is a unit of graphic information that defines a point in three-dimensional space.

Snake is an active contour which starts from an initial position and shape and fits itself to the shape of the desired object(s). Region growing schemes are well-known for providing a good estimation of object shape and boundary. Snake and Region Growing models utilize a closed contour to approach the object boundary by iteratively minimizing an energy function. One of the drawbacks of traditional contour schemes is that they often require human interaction and the segmentation results are heavily sensitive to initial seed points or region(s). A challenging issue in these CAD systems is choosing robust seed points or regions without user interaction. Several studies propose pre-processing algorithms such as evaluating threshold value(s) [12] or Gradient Vector Flow [13] to obtain proper seeds inside the lung.

The watershed algorithm is a powerful region-based method to segment images without the seed for initial contours or user interaction. This method is based on the phenomenon observed in geography that when water floods an area with hills and valleys, the water fills the lowest valleys first. Watershed methods tend to have relatively low computational cost. However, *over-segmentation* is a well-known drawback of watershed transformation. Therefore utilizing marker-based watershed transformation is suggested to overcome over-segmentation in the processing of medical images. However, collapsed lung would not be included with the lung voxels by the watershed transformation since these voxels have relatively high intensity, close to that of soft tissue.

Points of sharp variation are often among the most important features for analyzing the properties of transient signals or images. They are generally located at the boundaries of important image structures. Conventional edge detection algorithms are typically based on differential operators, such as the Sobel, Prewitt, and Roberts operators. Traditional differential operators work well with edge detection of noiseless images, however in the presence of noise may miss the edges or detect false edges due to their high level of sensitivity to noise and the existence of tiny intensity discontinuities in medical images. We have chosen to use wavelet transformation for the segmentation. Wavelet expansion in higher scales suppress the effect of noise on the edge detection process. It detects signal discontinuities if the basis function is chosen as a derivative of a proper smoothing function. Sharp transitions are depicted extremely well in wavelet expansions. Wavelet theory proves that discontinuities can be determined from the evolution across scales of the wavelet transform modulus maxima [14]; even the smoothness of an edge can be estimated from the decay of the wavelet transform maxima across scales.

A. wavelet transformation

Wavelet transformation represents a signal/image in multi-scale details by applying a basis function to the signal. The wavelet transform is capable of providing the spatial and frequency information simultaneously. Wavelets are families of functions $\Lambda_{s,t}(x)$ generated from a single base wavelet,

called the mother wavelet, $\Lambda(x)$ by dilations and translations

$$\Lambda_{s,t}(x) = \frac{1}{\sqrt{|s|}}\Lambda(\frac{x-t}{s}), \quad (1)$$

where s is the dilation (scale) parameter, and t is the translation parameter. Wavelets must have a mean of zero, and the useful ones have localized support in both spatial and Fourier domains.

We use the term 2D smoothing function to describe any function $\theta(x, y)$ whose integral over x and y is equal to 1 and converges to 0 at infinity. In the particular case where $\theta(x, y)$ is a Gaussian, the zero-crossing detection is equivalent to a Marr-Hildreth [15] edge detection, whereas the extrema detection corresponds to a Canny [16] edge detection. The image $f(x, y)$ is smoothed at different scales 's' by a convolution with $\theta(x, y)$. When the scale 's' is large, the convolution with $\theta_s(x, y)$ removes small signal fluctuations; therefore only the sharp variations of large structures will be detected. Edges are defined as points (x_0, y_0) where the modulus of the gradient vector is maximum in the direction towards which the gradient vector points in the image plane. In other words, edge points are inflection points of the surface $\nabla(f*\theta_s)(x, y)$. The direction of the gradient vector, $\nabla(f * \theta_s)(x, y)$, at a point (x_0, y_0) indicates the direction in the image plane (x, y) along which the directional derivative of $f(x, y)$ has the largest absolute value. Two wavelet functions $\Lambda^1_s(x, y)$ and $\Lambda^2_s(x, y)$ were defined such that

$$\begin{aligned} \Lambda^1_s(x, y) &= \frac{\partial\theta_s(x, y)}{\partial x} \\ \Lambda^2_s(x, y) &= \frac{\partial\theta_s(x, y)}{\partial y} \end{aligned} \quad (2)$$

The wavelet transform of $f(x, y)$ at scale 's' has two components, $W^1_s f$ and $W^2_s f$, defined by

$$\begin{aligned} W^1_s f(x, y) &= f * \Lambda^1_s(x, y) \\ W^2_s f(x, y) &= f * \Lambda^2_s(x, y) \end{aligned} \quad (3)$$

Usually, the wavelet model is not required to keep a continuous scale parameter 's'. To allow fast numerical implementations, Mallat and Zhong, [14], imposed that the scale only varies along the dyadic sequence $(2^j)_{j\in Z}$. A nonorthogonal wavelet is designed to satisfy the required characteristic for detecting lung edges and suppressing noise in the CT images. The mother wavelets are calculated from first and second derivatives of the smoothing function, $\theta(x, y)$, which is basically a low pass filter in the Fourier domain.

Noise filtration in the wavelet domain is performed based on the fact that sharp edges have large amplitude over the dyadic scales $(2^j, j = 0, 1, 2, ...)$, and noise dies out swiftly while 's' increases. The wavelet transform content at several adjacent scales was used to accurately detect the location of edges and some other fine details. If the first derivative of a smoothing function is chosen as the mother wavelet, the edges will be distinguished as local maxima points. Therefore, by increasing the scale, only significant maxima, which represent the edge pixels, will remain over the wavelet transformation and noise will be suppressed on these scales. In the case of choosing the second derivative of a smoothing function as the mother wavelet, the zero crossing will be considered as the location of the edges through the scales. However, considering the zero crossing will produce false edges since every singularity in the image leads to a zero crossing. Therefore other information should be combined with the zero crossings in order to distinguish between significant discontinuities and insignificant ones.

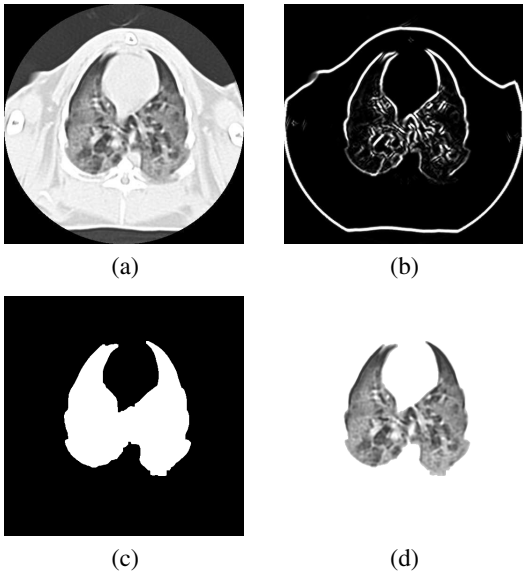

Fig. 2. (a) An original CT thorax image. (b) 2D wavelet transformation; multiplication of third and fourth scales (c) obtained mask (d) Extracted lung.

B. image processing

An inflection point of an image can either be a maximum or a minimum of the absolute value of its first derivative. The maxima of the absolute value of the first derivative are sharp variation points of image, whereas the lower values correspond to slower variations. The proposed method employed derivative of a smoothing function as its mother wavelet. Therefore maxima of the wavelet transformation magnitude were considered as candidates of edge points. In CT images, air-filled lung will appear with low intensities while the chest wall, blood, and bone will be higher. Therefore the border between the lung and adjacent tissues is represented as significant discontinuity in the image. Before transforming the image, voxels with HU value higher than the average body value were trimmed to avoid the detection of discontinuities between the bones and their adjacent soft body tissues. Each image was transformed into its dyadic scales. We found that considering dyadic scales between third and fifth provides necessary information for the edge points detection. Figure 2 (a) and (b) show an original image and multiplication of its transformation at third and fourth scales. Each scale is normalized and combined with other scales to extract the sharp variation points. Combination

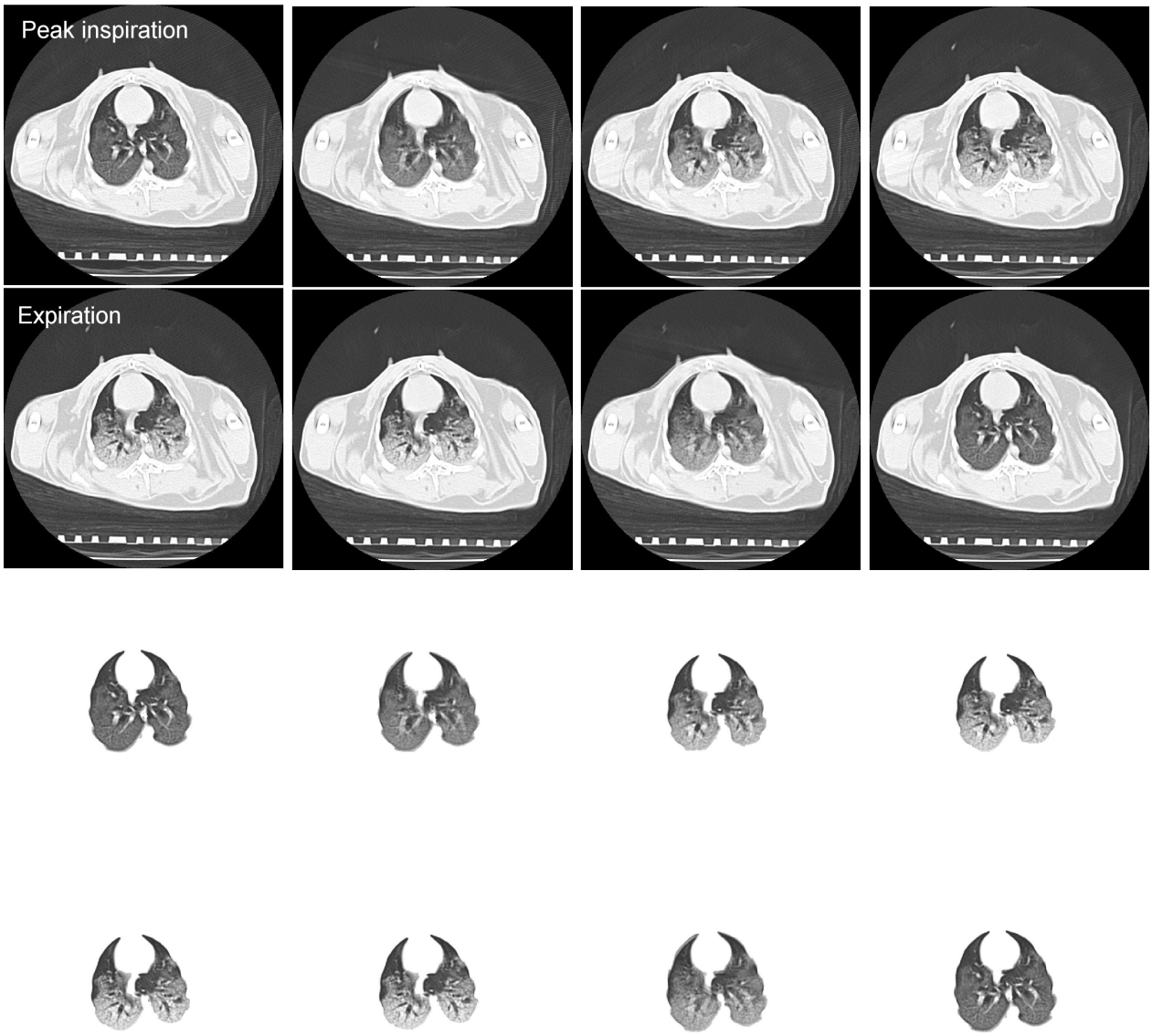

Fig. 3. The same thoracic level over a single respiratory cycle along with extracted lung consist of a series of 8 scans separated temporally by 0.4Sec.

of wavelet transformation in third and fourth scales is shown in figure 2 (b). The chest wall can be eliminated easily from the edge map since it has strong edges and is the closest continued object to the image border. After elimination of chest wall and all the surrounding objects, the remaining object with strong continued edges is lung. Maxima of the transformations and their directions ($argument(W_s^1 f + iW_s^2 f)$) was considered to evaluate the final edge map. Consequently the edge detection confined by constrain on continuity of the edge points. Figure 2 (c) and (d) illustrates the segmentation mask and extracted lung.

Dynamic CT with a cine loop technique was performed on a rabbit model with ARDS induced by repeated saline lavage. Dynamic CT was performed on an 8 detector multislice CT scanner (GE Lightspeed, GE Medical Systems, Milwaukee,WI). Imaging consisted of simultaneous acquisition of 4 slices (one volume) every 0.2 seconds. Images were acquired for just under 10 seconds producing 192 images per scan. The tube voltage was 120 kV and the tube current was 120 mA. A 512×512 matrix was used and the slice thickness was 5mm. The display field of view was 16cm. The voxel size was $0.3125 \times 0.3125 \times 5$mm with an average slice volume

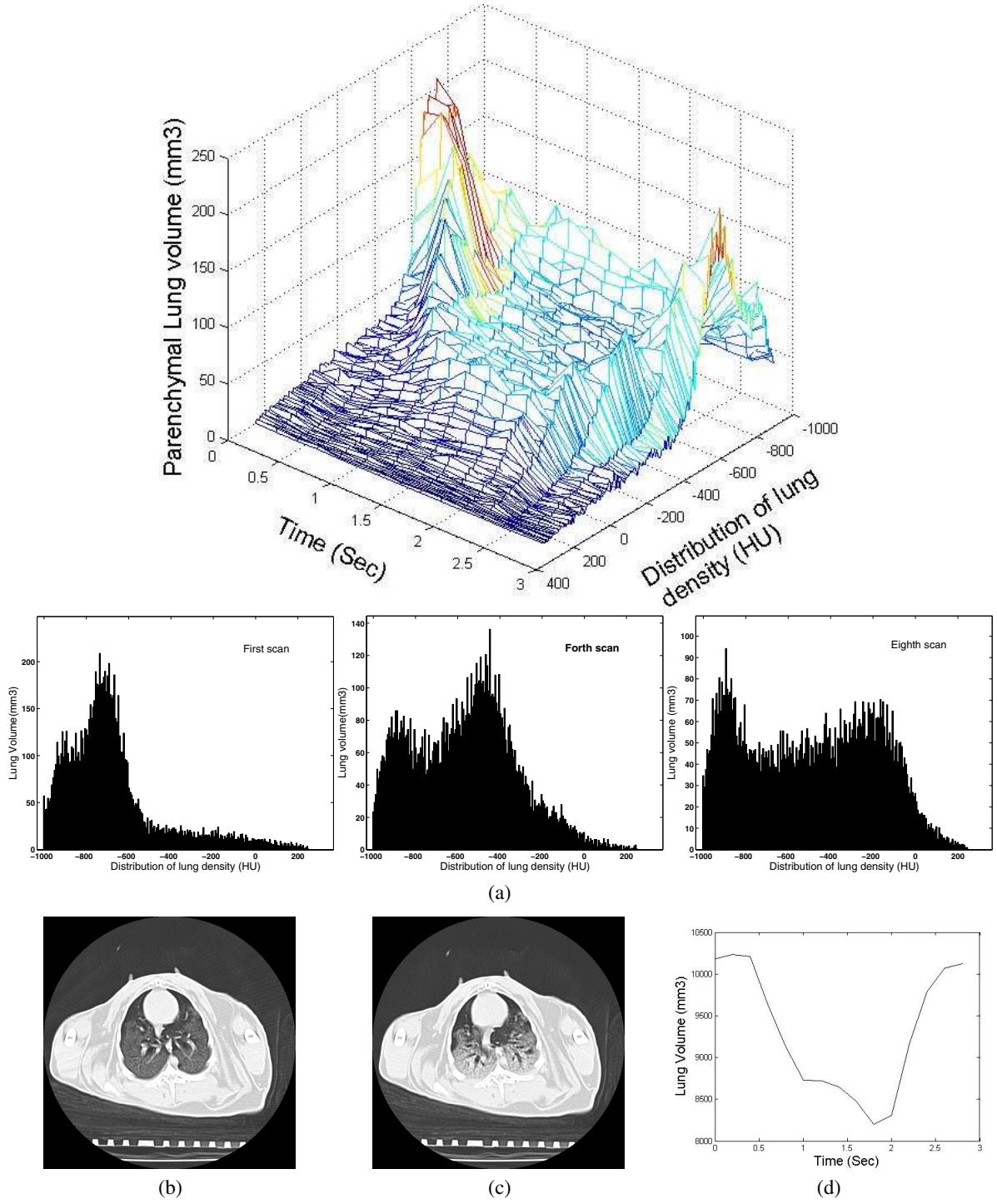

Fig. 4. (a) The same thoracic level over a single respiratory cycle consist of a series of 15 scans separated temporally by 0.2Sec. (b) Thoracic image at peak inspiration (time=0Sec) (c) Thoracic image at peak expiration (time=1.5Sec). (d) Lung volume vs. time over a single respiratory cycle.

of $128cm^2$. Use of between 4 and 6 volumes of 4 slices each enabled imaging of the whole chest throughout the respiratory cycle. Therefore each animal generated a dataset of between 768 (192×4) and 1152 (192×6) images. Images were reconstructed using a bone detail algorithm for lung visualization. In this study the rabbit lung segmented over

each respiratory cycle (Figure 3) and density occupied by substances with different HU values were calculated (Figure 4(a)). Automated segmented images compared with manually segmented images by an experienced radiologist to verify accuracy of the proposed method. A close correlation was found between the segmentation results. The volume between these segmentation calculated as system error. The average segmentation error calculated as $1mm^3$ in a respiration cycle.

III. DISCUSSION

Dynamic CT with a cine loop technique generates multiple scans of the same area of lung over a defined time period with 100 to 200 milliseconds between scans. This produces a movie of the lung over the respiratory cycle and enables a non-invasive and physiological study of ventilation without the need for breath-holding. However this technique produces a very large number of images for analysis with a single experiment generating several thousand images. An automated platform was developed which is capable of measuring the density occupied by substances with different HU values. Calculated volumes over a respiratory cycle are illustrated in figure 4. A program was developed in a MATLAB platform based on the proposed methodology to evaluate the CT images. The program processed each image in size of 512×512 within 2sec on a computer with 1.73GHz processor and 512MB RAM compared with several minutes for currently available manual segmentation software. Furthermore, the segmentation result is user adjustable as needed. Traditionally the volumes were measured by human interaction. This previous method lacked accuracy and consistency due to human error. Our newly developed method has brought speed and robustness to lung segmentation and lung density analysis.

Dynamic CT has many potential applications. As we have already described it may be used to assess changes in lung attenuation with time which occur in ARDS and to assess the effect of different therapeutic interventions in this condition. Changes in lung attenuation may also be used to assess diseases in which air trapping is an important feature such as emphysema and asthma [17]. Similarly, in foreign body aspiration it may be used to infer the location of the foreign body by identifying a region of lung which does not change in volume with respiration. Dynamic CT can also be used to look at patterns of contrast enhancement with time. This may be useful in the characterization of solitary pulmonary nodules (benign vs malignant) [18] and has also been shown to enable the characterization of different types of pulmonary edema [19]. A further potential application of dynamic CT is the assessment of diaphragmatic movement which may be abnormal in both neurological disorders and respiratory disease. Finally, dynamic ventilation imaging with four-dimensional pulmonary CT has recently been proposed as a way of examining regional ventilation as an aid to radiotherapy planning for lung cancer [20].

REFERENCES

[1] S. Szpala, M. Wierzbicki, G. Guiraudon, and T. M. Peters, "Real-time fusion of endoscopic views with dynamic 3-d cardiac images: A phantom study," *IEEE Transactions on Medical Imaging*, 2005.

[2] C. Chen and T. Huang, "Analysis of left ventricle global deformation based on dynamic CT data," in *11th IAPR International Conference on Pattern Recognition*, 1992.

[3] L. Gu, "Hybrid 3d heart segmentation from dynamic CT images," in *IEEE/EMBS International Summer School on Medical Devices and Biosensors*, 2004.

[4] N. Takagi, Y.Kawata, N. Niki, K.Mori, H.Ohmatsu, R.Kakinuma, K. Eguchi, M. Kusumoto, M. Kaneko, and N. Moriyama, "3d analysis of solitary pulmonary nodules based on contrast enhanced dynamic CT," in *International Conference on Image Processing*, 1999.

[5] H. Kim, K. Lee, E. Kang, G. Y. Suh, O. J. Kwon, and M. J. Chung, "Acute respiratory distress syndrome computed tomography findings and their applications to mechanical ventilation therapy," *Journal of Computer Assisted Tomography*, 2004.

[6] J. Rouby, L. Puybasset, P. Cluzel, J. Richecoeur, Q. Lu, and P. Grenier, "Regional distribution of gas and tissue in acute respiratory distress syndrome: Ii. physiological correlation and definition of an ARDS severity score," *Intensive Care Med.*, 2000.

[7] T. Luecke, P. Herrman, P. Kraincuk, and P. Pelosi, "Computed tomography scan assessment of lung volume and recruitment during high-frequency oscillatory ventilation," *Crit Care Med*, 2005.

[8] L. Gattinoni, P. Caironi, P. Pelosi, and L. Goodman, "What has computed tomography taught us about the acute respiratory distress syndrome," *Am J Respir Crit Care Med.*, 2001.

[9] K. Markstaller, H. Kauczor, N. Weiler, J. Karmrodt, M. Doebrich, M. Ferrante, M. Thelen, and B. Eberle, "Lung density distribution in dynamic CT correlates with oxygenation in ventilated pigs with lavage ARDS," *Br J Anaesth*, 2003.

[10] S. Hu, E. A. Hoffman, and J. M. Reinhardt, "Automatic lung segmentation for accurate quantitation of volumetric x-ray CT images," in *Medical Imaging, IEEE Transactions*, vol. 20, 2001, pp. 490 – 498.

[11] S. N. Yu and C. T. Chiang, "Similarity searching for chest CT images based on object features and spatial relation maps," in *Engineering in Medicine and Biology Society, EMBC*, vol. 1, 2004, pp. 1298 – 1301.

[12] Y. Itai, K. Hyoungseop, S. Ishikawa, S. Katsuragawa, K. N. T. Ishida, and A. Yamamoto, "Automatic segmentation of lung areas based on snakes and extraction of abnormal areas," in *Tools with Artificial Intelligence, ICTAI 05. 17th IEEE International Conference*, 2005, pp. 377 – 381.

[13] C. H. Chuang and W. N. Lie, "Region growing based on extended gradient vector flow field model for multiple objects segmentation," in *Image Processing, International Conference*, vol. 3, 2001, pp. 74 – 77.

[14] S. Mallat and S. Zhong, "Characterization of signals from multiscale edges," in *Pattern Analysis and Machine Intelligence*, vol. 14, 1992, pp. 710 – 732.

[15] D. Marr, *Vision*. San Francisco: W.H. Freeman, 1982.

[16] J. Canny, "A computational approach to edge detection," in *IEEE Transactions on Pattern Analysis and Machine Intelligence*, vol. PAMI-8, 1986, pp. 679–698.

[17] R. Tanaka, S. Sanada, N. Okazaki, T. Kobayashi, M. Fujimura, M. Yasui, T. Matsui, K. Nakayama, Y. Nanbu, and O. Matsui, "Evaluation of pulmonary function using breathing chest radiography with a dynamic flat panel detector: primary results in pulmonary diseases," *Invest Radiol*, vol. 41, 2006.

[18] C. Yi, K. Lee, E. Kim, J. Han, H. Kim, O. Kwon, Y. Jeong, and S. Kim, "Solitary pulmonary nodules: Dynamic enhanced multi-detector row CT study and comparison with vascular endothelial growth factor and microvessel density," *Radiology*, vol. 233, 2004.

[19] C. Schueller-Weidekamm, E. Wassermann, H. Redl, M. Prokop, M. Zimpfer, C. Herold, P. Germann, and R. Ullrich, "Dynamic CT measurement of pulmonary enhancement in piglets with experimental acute respiratory distress syndrome," *Radiology*, vol. 239, 2006.

[20] T. Guerrero, K. Sanders, E. Castillo, Y. Zhang, L. Bidaut, T. Pan, and R. Komaki, "Dynamic ventilation imaging from four-dimensional computer tomography," *Phys Med Biol*, vol. 51, 2006.